



HAL
open science

Decomposing a prior-CT-based cone-beam CT projection correction algorithm into scatter and beam hardening components

Christoph Zöllner, Simon Rit, Christopher Kurz, Gloria Vilches-Freixas, Florian Kamp, George Dedes, Claus Belka, Katia Parodi, Guillaume Landry

► **To cite this version:**

Christoph Zöllner, Simon Rit, Christopher Kurz, Gloria Vilches-Freixas, Florian Kamp, et al.. Decomposing a prior-CT-based cone-beam CT projection correction algorithm into scatter and beam hardening components. *Physics and Imaging in Radiation Oncology*, 2017, 3, pp.49 - 52. 10.1016/j.phro.2017.09.002 . hal-01743232

HAL Id: hal-01743232

<https://hal.science/hal-01743232>

Submitted on 26 Mar 2018

HAL is a multi-disciplinary open access archive for the deposit and dissemination of scientific research documents, whether they are published or not. The documents may come from teaching and research institutions in France or abroad, or from public or private research centers.

L'archive ouverte pluridisciplinaire **HAL**, est destinée au dépôt et à la diffusion de documents scientifiques de niveau recherche, publiés ou non, émanant des établissements d'enseignement et de recherche français ou étrangers, des laboratoires publics ou privés.



Technical Note

Decomposing a prior-CT-based cone-beam CT projection correction algorithm into scatter and beam hardening components



Christoph Zöllner^a, Simon Rit^b, Christopher Kurz^{a,c,d}, Gloria Vilches-Freixas^b, Florian Kamp^{c,d}, George Dedes^a, Claus Belka^{c,d}, Katia Parodi^a, Guillaume Landry^{a,*}

^a Department of Medical Physics, Faculty of Physics, Ludwig-Maximilians-Universität München (LMU Munich), Am Coulombwall 1, 85748 Garching, Germany

^b Univ Lyon, INSA-Lyon, Université Claude Bernard Lyon 1, UJM-Saint Étienne, CNRS, Inserm, CREATIS UMR 5220, U1206, Centre Léon Bérard, F-69373 Lyon, France

^c Department of Radiation Oncology, University Hospital, LMU Munich, Munich, Germany

^d German Cancer Consortium (DKTK), Munich, Germany

ARTICLE INFO

Keywords:

CBCT
Scatter
Monte Carlo
Beam hardening
Proton therapy

ABSTRACT

A scatter correction algorithm (SCA) for cone beam CT (CBCT) projections, making use of prior information obtained by deformable image registration of CT to CBCT, has recently been proposed and tested for particle therapy dose calculation. The SCA relies on subtraction of digitally reconstructed radiographs (DRR) from scaled measured projections and smoothing operations, followed by a subtraction correction and reconstruction. In this note, we compared the SCA's correction to one based on a Monte Carlo simulation of the scatter, and a separate beam hardening correction. Agreement better than 3% between the two approaches was obtained when comparing corrected log-transformed projections.

1. Introduction

Cone beam computed tomography (CBCT) image guidance for proton therapy (PT) has recently seen considerable interest, with several PT centers either planning to deploy or making use of gantry-, nozzle-, C-arm- or couch-mounted systems. While the images obtained from these systems are chiefly used for patient positioning, there is interest in using them for water equivalent thickness (WET) or dose calculation purposes, which require correction of CBCT image intensities. CT number conversion is problematic due to the lack of a single bijective relation between directly reconstructed CBCT Hounsfield units and stopping power ratio [1], and requires improvement of CBCT image quality [2]. Recent studies have adopted methods initially applied to photon therapy [3–5] to achieve CBCT correction for PT by relying on deformable image registration of a planning CT to the CBCT to yield a so-called virtual CT (vCT) [1,6–11]. An algorithm making use of digitally reconstructed radiographs (DRR) of the vCT to perform corrections directly on CBCT projection images [12,13] has recently been successfully tested for PT [14]. This so-called scatter-correction-algorithm (SCA) is reported equivalent to the vCT approach for head and neck sites and superior for pelvic sites in terms of WET, dose calculations or organ at risk delineation [15]. In the original papers from Niu et al. [12,13], as well as in the PT-specific reports of Park et al. and Kurz et al. [14,15], it is stated that the SCA not only corrects

for the detection of scattered photons by the flat panel imager, but also for any other sources of low-frequency discrepancies between the vCT and the CBCT. This may be other artefacts, e.g., beam hardening, but it might as well be image properties, e.g., the use of different X-ray tube voltages. There is thus a concern that the algorithm could be too strongly influenced by the prior information and yield unphysical scatter correction.

In this note, we performed Monte Carlo (MC) simulation of a CBCT projection for comparison against a measured projection. We compared the SCA's correction to one based solely on MC results using the scatter component from the MC simulation and a separate beam hardening correction. Our objective was to assess whether the SCA's correction can be reproduced by independent scatter and beam hardening corrections.

2. Materials and methods

2.1. Data acquisition

A 15 cm diameter PMMA cylinder with a central bore housing four Gammex RMI 467 inserts (lung LN450, solid water, adipose AP6 and bone SB3, Gammex, USA) was imaged with the S20 protocol of the XVI 4.5.1 CBCT imaging system of an Elekta Synergy linac (Elekta, Sweden). The scanner was operated at 100 kVp using a tube current of

* Corresponding author.

E-mail address: g.landry@lmu.de (G. Landry).

10 mA, an exposure time of 10 ms/projection, 391 projections and no bow-tie filter. A 180 degrees plus fan angle rotation was performed. Uncorrected flood, dark and phantom projections of 1024×1024 pixels, subsequently re-binned to 512×512 0.8×0.8 mm² pixels were acquired with a frame-grabber card (PerkinElmer, USA) connected to the flat panel imager, yielding pixel signals ranging to 2^{16} (the limit of unsigned 16-bits integers used for file writing). Phantom projections I_{CBCT} were obtained following dark and flood correction (see [Supplementary materials Eq. \(S1\)](#) for details).

CBCT images were reconstructed from I_{CBCT} following log transformation to projections

$$p = -\ln(I_{CBCT}/I_0), \quad (2)$$

where I_0 corresponds to I_{CBCT} without an object. CBCT images μ_{CBCT} were reconstructed on a $1 \times 1 \times 1$ mm³ voxel grid with the reconstruction toolkit (RTK) [16] from the set of p and converted to CT numbers (CT#) as in Park et al. [14]:

$$CT\#_{CBCT} = \mu_{CBCT} \times 2^{16} - 1024, \quad (3)$$

where $CT\# = (\mu - \mu_{water})/\mu_{water} \times 1000$ in Hounsfield units (HU) and μ is the linear attenuation coefficient. The phantom was also scanned with a Toshiba Aquilion LB scanner (Toshiba Medical Systems, the Netherlands) at 120 kVp, using clinical scan protocols for treatment planning, and images were reconstructed on a $1 \times 1 \times 3$ mm³ voxel grid and rigidly registered to the CBCT image. The use of deformable image registration was not necessary in this study.

2.2. SCA algorithm

The SCA algorithm as implemented in this work is described in details in Park et al. and Kurz et al. [14,15], and a short three steps overview is presented below.

Step 1: The CBCT measurements (dark and gain corrected detector signals before log transformation) I_{CBCT} were processed with the SCA algorithm where the SCA correction I_{SCA} is first calculated with:

$$I_{SCA} = f(CF \times I_{CBCT} - I_{DRR}), \quad (4)$$

where I_{DRR} were the DRRs of the prior CT# image in the same geometry as the CBCT projections, following conversion to scaled photon attenuation by inverting Eq. (3): $\mu_{CT} = (CT\# + 1024)/2^{16}$ and $I_{DRR} = 2^{16}e^{-DRR}$. f was a smoothing operation consisting of a 2D median filter with 25×25 pixels size followed by a Gaussian filter of 1.5 pixel standard deviation [12]. $CF = mAs_{ref}/mAs$, with $mAs_{ref} = 2.56$ mAs was an empirically derived correction factor introduced by Park et al. [14] and validated in Kurz et al. [15]. The CF was meant to adjust CBCT and CT projection intensities so that their difference yields a correct I_{SCA} , and additionally accounts for different mAs/projection between imaging protocols.

Step 2: SCA corrected detector signals were obtained by:

$$I_{cor,SCA} = CF \times I_{CBCT} - I_{SCA}. \quad (5)$$

Step 3: Reconstruction of these projections following log transform as per Eq. (2) and conversion with Eq. (3) yielded a corrected CBCT image ($CBCT_{cor,SCA}$).

The extensive validation for phantoms and patient data in terms of image quality of the SCA was reported in Park et al. and Kurz et al. [14,15]. The generous filtering in the SCA results in the removal of low-frequency mismatches between scaled CBCT projections and DRRs due to the detection of scattered photons and beam hardening effects.

2.3. MC simulation and estimation of scatter

We performed MC simulation of the CBCT projection acquisition using the fixed forced detection actor of the GATE MC simulation toolkit [17], based on the approach of Poludniowski et al. [18]. In this framework, the primary photon intensity reaching the detector was

calculated by raytracing from a point source to each detector element through a voxelized representation of the phantom accounting for the material specific energy dependence of μ . The X-ray spectrum and detector energy response of the XVI system were obtained from an optimization procedure performed by Vilches-Freixas et al. [19] following the approach of Granton et al. [20]. The CT scan of the phantom was used to generate its voxelized representation in GATE by converting the CT# to the densities and material compositions of the four inserts and PMMA reported by the manufacturer. The primary signal from MC was labelled P_{MC} . A full MC simulation using Geant4's low energy electromagnetic physics models was run to record scatter events in the phantom (first, second, etc.). For each scatter event, the probability of scattered photons reaching each detector pixel was calculated using raytracing accounting for attenuation, the detector's energy response and angular and energy differential scattering cross sections. This yielded the scatter signal S_{MC} . The simulation geometry was matched to the CBCT acquisition, however a coarser projection grid (128×128) was used for scatter detection, requiring interpolation and scaling before addition to the primary signal. The combined MC detector signal $I_{MC} = P_{MC} + S_{MC}$ was converted to $I_{CBCT,MC}$ using the following:

$$I_{CBCT,MC} = 2^{16} \times I_{MC} \times \frac{\text{median}(I_{flood,MC})}{I_{flood,MC}} \quad (6)$$

where I_{MC} was the sum of the primary and scattered signals and $I_{flood,MC}$ was the object-free primary signal.

Given the cylindrical symmetry of our phantom and to avoid modelling the patient table and phantom support, the scatter component of a single projection where the table was out of the FOV was computed with Monte Carlo simulations in this work. However, all I_{SCA} projections were computed and used to reconstruct $CBCT_{cor,SCA}$, as well as all primary projections calculated with GATE to reconstruct the scatter-less CBCT.

2.4. Beam hardening correction

The log transformed MC primary signal $-\ln(P_{MC}/I_{flood,MC})$ was used to establish the conversion between scatter-free CBCT projections and DRRs of μ_{CT} by performing beam hardening and μ scaling (necessary due to the different kVp between CT and CBCT) in one step. This was done by fitting a quadratic relationship between $-\ln(P_{MC}/I_{flood,MC})$ and DRRs of μ_{CT} , assuming the CT was corrected for beam hardening, in a similar approach to Thing et al. [2]. This is illustrated in [Fig. S1 of the supplementary materials](#). The fitting function converting MC primary log projections to DRRs was labelled F_{BH} .

2.5. Independent scatter and beam hardening corrections

We additionally calculated $S_{CBCT,MC}$ by substituting I_{MC} by S_{MC} in Eq. (6). This was used to calculate

$$-\ln(I_{cor,MC}/I_0) = F_{BH}[-\ln[(I_{CBCT} - S_{CBCT,MC})/I_0]], \quad (7)$$

which would yield a MC corrected $CBCT_{cor,MC}$. This image was however not reconstructed in this work, given the aforementioned lack of patient table modelling for all projections. The projection from Eq. (7) was used to benchmark the SCA's corrected projection (replacing I_{CBCT} in Eq. (2) by $I_{cor,SCA}$ from Eq. (5)).

3. Results

In [Fig. 1](#), a measured log transformed projection is compared to the one obtained from the MC simulation. For all inserts the agreement was generally good, with the largest discrepancy behind the bone insert (maximum 3%, [Fig. 1A](#)). [Fig. 1](#) additionally shows $-\ln(I_{cor,SCA}/I_0)$ and $-\ln(I_{cor,MC}/I_0)$ where similar good agreement was observed. The largest difference between the two correction methods was 3% behind the

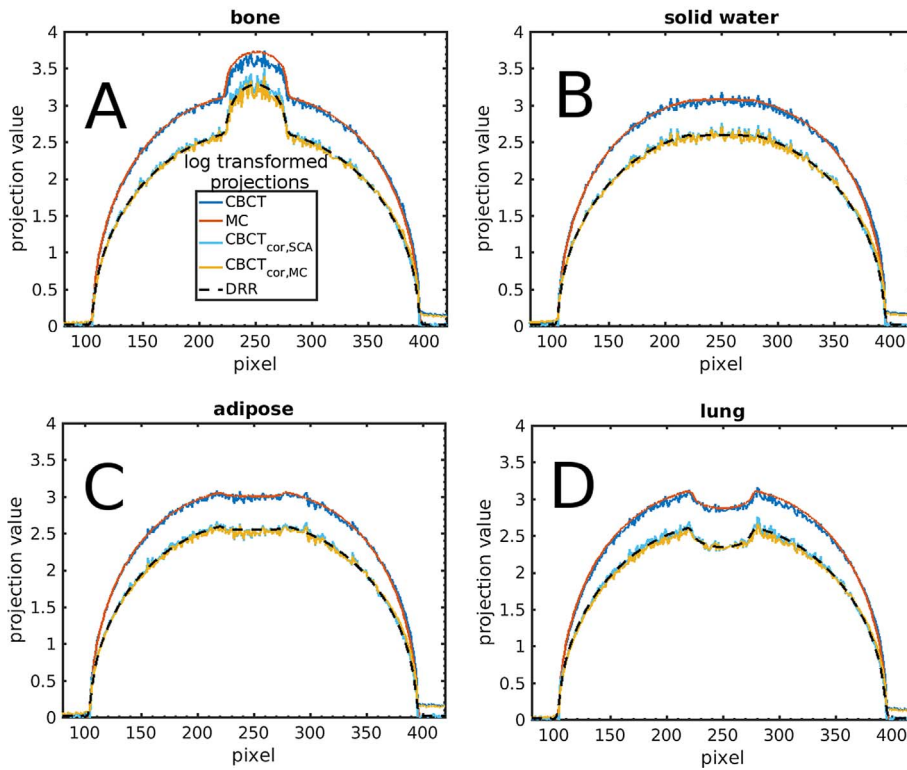


Fig. 1. Comparison of log transformed projections measured by the flat panel detector (CBCT) and obtained from MC simulations (MC) along a profile across the phantom diameter centered on (A) the bone, (B) the solid water, (C) the adipose and (D) the lung inserts. The DRR from the planning CT is shown along with log transformed $I_{cor,SCA}$ from the SCA (CBCT_{cor,SCA}) and using the MC derived scatter signal to obtain $I_{cor,MC}$ (CBCT_{cor,MC}).

bone insert, similar to the MC vs CBCT residual error for uncorrected projections.

In Fig. 2, the CT and CBCT_{cor,SCA} images (in CT#) are compared for the bone insert to show the impact of incorrect CT beam hardening correction on the CBCT_{cor,SCA}. We observed a residual cupping artefact on the CT image attributed to incomplete beam hardening correction from the vendor software. This artefact seemed to have been propagated to the CBCT_{cor,SCA}. For comparison, the MC primary projection was also corrected for beam hardening using the correction derived in this work and reconstructed. A similar residual cupping artefact was observed (see Fig. 2), suggesting that our beam hardening correction may suffer from similar shortcomings as the vendor’s.

In the Supplementary material, the intensity of the scatter component of the projections, as derived from the SCA and from MC, was also compared and their absolute average difference relative to the MC in a projection was 3% (Supplementary Fig. S2). The bone insert showed the largest residual mismatch with an average difference of 12%. In Supplementary material, the reconstructed CT, CBCT and CBCT_{cor} images are shown (Fig. S3) in addition to a table (Table S1) reporting

mean CT# inside regions of interest covering each insert. The largest linear attenuation coefficient (converting CT# to μ/μ_{water}) discrepancy was 1.5% for the bone insert.

4. Discussion

The good agreement between simulations and measurements shown in Fig. 1 supports the optimization work of Vilches-Freixas et al. [19], which relied on the technique proposed by Granton et al. [20]. The mismatch visible beyond pixel 400 is caused by the foam phantom holder which was not modeled in the MC simulation. The results shown in Fig. 1, with accuracy better than 3%, are an indirect indication, since scatter was not measured directly, that the MC calculated S_{MC} should be reasonably accurate. This level of accuracy compares well to what was achieved in other MC studies such as Bootsma et al. [21] (6%) or Jarry et al. [22] (8–10%).

The agreement between the corrected log transformed projections shown in Fig. 1 (largest difference 3%) indicates that the main corrections of the SCA are indeed for scatter and beam hardening, as

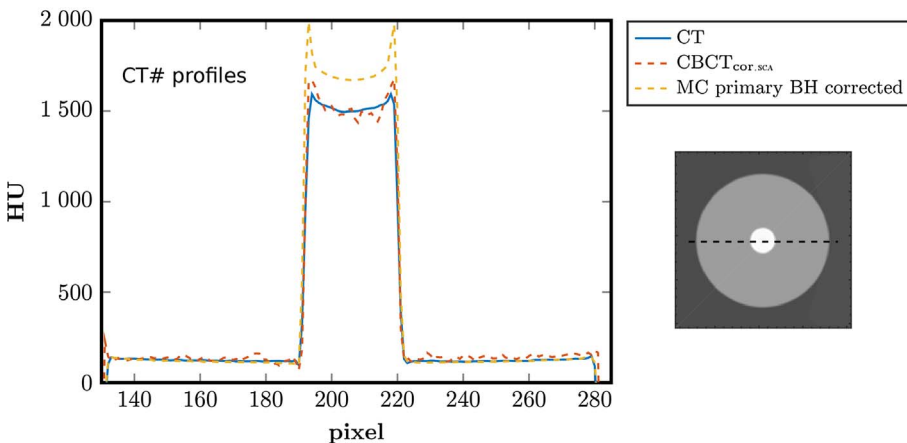


Fig. 2. Profiles across the CT and CBCT_{cor,SCA} images are shown for the bone insert along the dashed line shown on the CT image. The reconstructed beam hardening corrected MC primary is also shown for comparison. Note that CBCT_{cor,MC} was not reconstructed because only one projection was simulated in this work since the table and phantom holder were not simulated.

suggested in Niu et al. [12,13] and Park et al. [14]. However, it is obvious from Fig. 2 that the SCA may potentially propagate residual artefacts present in the CT image in the $CBCT_{cor,SCA}$. The residual cupping in the reconstructed beam-hardening-corrected MC primary suggests that the one-material correction used in this work would also yield artefacts in MC-corrected CBCT projections. The slight mismatch in CT numbers in the bone insert between the CT and MC data in Fig. 2 is also attributed to the PMMA-specific beam hardening correction.

The log-transformed projections agreement of Fig. 1, given the relative importance of scatter and primary, masks the magnitude of the difference between the scatter intensity estimated by the SCA after removing the beam hardening correction and that from MC simulation, which was up to 12% behind the bone insert (see Supplementary material Fig. S2). Other studies have found comparable levels of agreement between MC simulation and measurements, such as Bootsma et al. reporting 3%–14% between MC and measured scatter to primary ratio for water cylinders [21] or Chen et al. reporting 5% agreement for a breast phantom [23].

The residual discrepancies in scatter intensity estimation can be partly attributed to discrepancies in the MC modelling and to the material specificity of the beam hardening correction, since most data points are from PMMA or PMMA + adipose in the beam hardening fit (see Fig. S1 in supplementary materials). Since the CT is acquired at a different kVp and knowledge of the vendor's beam hardening correction is incomplete, it is clear that our single-material correction cannot be accurate for all materials; the largest discrepancy is behind bone which is the most different to PMMA in terms of elemental composition (effective atomic number 14 vs 6.7, respectively).

A water based beam hardening correction could have been obtained using the knowledge of the CBCT X-ray spectrum and detector energy response from our MC simulations to linearize the CBCT attenuation. However a second step converting the 100 kVp CBCT attenuation to the 120 kVp CT attenuation would have still been necessary for comparison against the SCA's results. We chose the PMMA empirical correction from MC CBCT primary to CT DRR to avoid relying on knowledge of the CT scanner spectrum and detector response.

In conclusion, we have shown, making use of MC simulation, that the SCA correction can be reproduced to an accuracy of approximately 3% by performing separate scatter and beam hardening corrections derived from MC-based estimates. This indicates that the SCA's correction can be assumed to correspond to beam hardening and scatter corrections. However these conclusions may not hold for CT images containing severe artefacts or with geometry differing from the CBCT.

Acknowledgements

Jan Hofmaier, Michael Reiner and Abdulaziz Alhazmi are thanked for support related to CBCT projection acquisition. Yang-Kyun Park, Brian Winey and Greg Sharp are thanked for support with the implementation of the SCA. This project was partly funded by the German Research Foundation (DFG) Cluster of Excellence Munich-Centre for Advanced Photonics and the Federal Ministry of Education and Research of Germany (BMBF) grant No. 01IB13001 (SPARTA). The Bayerisch-Französisches Hochschulzentrum (BFHZ) is acknowledged for supporting travel between Munich and Lyon. This work was partially supported by grants ANR-13-IS03-0002-01 and ANR-14-CE23-0008 (DEXTER and t-Gate projects) from the French National Research Agency (ANR).

Appendix A. Supplementary data

Supplementary data associated with this article can be found, in the online version, at <http://dx.doi.org/10.1016/j.phro.2017.09.002>.

References

- [1] Kurz C, Dedes G, Resch A, et al. Comparing cone-beam CT intensity correction methods for dose recalculation in adaptive intensity-modulated photon and proton therapy for head and neck cancer. *Acta Oncol* 2015;54:1651–7.
- [2] Thing RS, Bernchou U, Mainegra-Hing E, Hansen O, Brink C. Hounsfield unit recovery in clinical cone beam CT images of the thorax acquired for image guided radiation therapy. *Phys Med Biol* 2016;61:5781–802.
- [3] Peroni M, Ciardo D, Spadea MF, et al. Automatic segmentation and online virtualCT in head-and-neck adaptive radiation therapy. *Int J Radiat Oncol Biol Phys* 2012;84:e427–33.
- [4] Veiga C, McClelland J, Moinuddin S, et al. Toward adaptive radiotherapy for head and neck patients: Feasibility study on using CT-to-CBCT deformable registration for “dose of the day” calculations. *Med Phys* 2014;41:031703.
- [5] Thing RS, Bernchou U, Hansen O, Brink C. Accuracy of dose calculation based on artefact corrected Cone Beam CT images of lung cancer patients. *Phys Imaging Radiat Oncol* 2017;1:6–11.
- [6] Landry G, Dedes G, Zollner C, et al. Phantom based evaluation of CT to CBCT image registration for proton therapy dose recalculation. *Phys Med Biol* 2015;60:595–613.
- [7] Landry G, Nijhuis R, Dedes G, et al. Investigating CT to CBCT image registration for head and neck proton therapy as a tool for daily dose recalculation. *Med Phys* 2015;42:1354–66.
- [8] Thomson DJ, Teo B-KK, Ong A, et al. The Impact of Anatomic Change on Pencil Beam Scanning in the Treatment of Oropharynx Cancer. *Int J Part Ther* 2015;2:394–403.
- [9] Veiga C, Alshaihi J, Amos R, et al. Cone-beam computed tomography and deformable registration-based “dose of the day” calculations for adaptive proton therapy. *Int J Part Ther* 2015;2:404–14.
- [10] Kurz C, Nijhuis R, Reiner M, et al. Feasibility of automated proton therapy plan adaptation for head and neck tumors using cone beam CT images. *Radiat Oncol* 2016;11:64.
- [11] Veiga C, Janssens G, Teng CL, et al. First clinical investigation of cone beam computed tomography and deformable registration for adaptive proton therapy for lung cancer. *Int J Radiat Oncol Biol Phys* 2016;95:549–59.
- [12] Niu T, Sun M, Star-Lack J, Gao H, Fan Q, Zhu L. Shading correction for on-board cone-beam CT in radiation therapy using planning MDCT images. *Med Phys* 2010;37:5395–406.
- [13] Niu T, Al-Basheer A, Zhu L. Quantitative cone-beam CT imaging in radiation therapy using planning CT as a prior: first patient studies. *Med Phys* 2012;39:1991–2000.
- [14] Park YK, Sharp GC, Phillips J, Winey BA. Proton dose calculation on scatter-corrected CBCT image: Feasibility study for adaptive proton therapy. *Med Phys* 2015;42:4449–59.
- [15] Kurz C, Kamp F, Park YK, et al. Investigating deformable image registration and scatter correction for CBCT-based dose calculation in adaptive IMPT. *Med Phys* 2016;43:5635.
- [16] Rit S, Oliva MV, Brousmiche S, Labarbe R, Sarrut D, Sharp GC. The Reconstruction Toolkit (RTK), an open-source cone-beam CT reconstruction toolkit based on the Insight Toolkit (ITK). *J Phys Conf Ser* 2014;489:012079.
- [17] Jan S, Santin G, Strul D, et al. GATE: a simulation toolkit for PET and SPECT. *Phys Med Biol* 2004;49:4543–61.
- [18] Poludniowski G, Evans P, Hansen V, Webb S. An efficient Monte Carlo-based algorithm for scatter correction in keV cone-beam CT. *Phys Med Biol* 2009;54:3847.
- [19] Vilches-Freixas G, Letang JM, Brousmiche S, et al. Technical Note: Procedure for the calibration and validation of kilo-voltage cone-beam CT models. *Med Phys* 2016;43:5199.
- [20] Granton PV, Podesta M, Landry G, Nijsten S, Bootsma G, Verhaegen F. A combined dose calculation and verification method for a small animal precision irradiator based on onboard imaging. *Med Phys* 2012;39:4155–66.
- [21] Bootsma GJ, Verhaegen F, Jaffray DA. The effects of compensator and imaging geometry on the distribution of x-ray scatter in CBCT. *Med Phys* 2011;38:897–914.
- [22] Jarry G, Graham SA, Moseley DJ, Jaffray DJ, Siewersden JH, Verhaegen F. Characterization of scattered radiation in kV CBCT images using Monte Carlo simulations. *Med Phys* 2006;33:4320–9.
- [23] Chen Y, Liu B, O'Connor JM, Didier CS, Glick SJ. Characterization of scatter in cone-beam CT breast imaging: comparison of experimental measurements and Monte Carlo simulation. *Med Phys* 2009;36:857–69.